

Anisotropic multimessenger signals from black hole neutrino-dominated accretion flows with outflows in binary compact object mergers

YAN-QING QI,¹ TONG LIU,^{1,2} BAO-QUAN HUANG,¹ YUN-FENG WEI,¹ AND DE-FU BU^{3,2}

¹*Department of Astronomy, Xiamen University, Xiamen, Fujian 361005, China*

²*SHAO-XMU Joint Center for Astrophysics, Xiamen University, Xiamen, Fujian 361005, China*

³*Key Laboratory for Research in Galaxies and Cosmology, Shanghai Astronomical Observatory, Chinese Academy of Sciences, Shanghai 200030, China*

ABSTRACT

A black hole (BH) hyperaccretion system might be born after the merger of a BH and a neutron star (NS) or a binary NS (BNS). In the case of a high mass accretion rate, the hyperaccretion disk is in a state of neutrino-dominated accretion flow (NDAF) and emits numerous anisotropic MeV neutrinos. Only a small fraction of these neutrinos annihilates in the space outside of the disk and then launch ultrarelativistic jets that break away from the merger ejecta to power gamma-ray bursts. Mergers and their remnants are generally considered sources of gravitational waves (GWs), neutrinos, and kilonovae. Anisotropic neutrino emission and anisotropic high-velocity material outflows from central BH-NDAF systems can also trigger strong GWs and luminous disk-outflow-driven (DOD) kilonovae, respectively. In this paper, the anisotropic multimessenger signals from NDAFs with outflows, including DOD kilonovae, MeV neutrinos, and GWs, are presented. As the results, the typical AB magnitude of the DOD kilonovae is lower than that of AT 2017gfo at the same distance, and it decreases with increasing viewing angles and its anisotropy is not sensitive to the outflow mass distribution but mainly determined by the velocity distribution. Since neutrinos with $\gtrsim 10$ MeV are mainly produced in the inner region of the disk, they will be dramatically deflected to a large viewing angle by relativity effects. Moreover, the strains of GWs induced by anisotropic neutrinos increase with increasing viewing angles. The accumulation of multimessenger detection of the BH-NS/BNS mergers with different viewing angles might further verify the existence of NDAFs with outflows.

Keywords: accretion, accretion disks - black hole physics - gamma-ray burst: general - gravitational waves - neutrinos

1. INTRODUCTION

In the era of multimessenger astronomy, the merger of a black hole (BH) and a neutron star (NS) or a binary NS (BNS) offers four mainly different probes, i.e., gamma-ray bursts (GRBs), kilonovae, neutrinos, and gravitational waves (GWs). As the binaries approach each other during the merger, some of their mass becomes tidally disrupted, forming a central compact object, which may be a magnetar (e.g., Duncan & Thompson 1992; Usov 1992; Zhang & Mészáros 2001; Dai et al. 2006) or a BH (e.g., Woosley 1993; Lei et al. 2009, 2013; Liu et al. 2017a). The inspiral and coalescence of compact objects are prime sources of GWs (e.g., Schutz

1989; Cutler & Flanagan 1994; Sathyaprakash & Schutz 2009; Abadie et al. 2010; Baiotti & Rezzolla 2017). The neutron-rich ejecta released from BNS/BH-NS mergers undergo a rapid neutron capture nucleosynthesis process (*r*-process) to power kilonovae (e.g., Li & Paczyński 1998; Kasen et al. 2013; Just et al. 2015; Metzger 2019; Nakar 2020; Cowan et al. 2021). During the postmerger dynamical time, some of the materials on the accretion disk are accreted into the central compact object and thus produce relativistic jets, which would be detected as GRBs if they point toward the Earth (e.g., Paczyński 1986; Eichler et al. 1989; Paczyński 1991; Narayan et al. 1992; Popham et al. 1999). Then, the interaction between the jet and the external medium might generate long-lasting X-ray, optical, and radio afterglows (e.g., Rees & Mészáros 1992; Berger et al. 2005; Nakar 2007; Berger 2014). In addition to GWs and electromag-

netic radiation, a tremendous number of neutrinos with $\gtrsim 10$ MeV are also expected to be emitted from the remnant of BNS/BH-NS mergers (e.g., Sekiguchi et al. 2011; Kyutoku & Kashiyaama 2018).

GW 170817, originating from a BNS merger, was detected by aLIGO and Virgo on August 17, 2017 (Abbott et al. 2017a). At ~ 1.7 s after the end of the inspiral, GRB 170817A was triggered independently by *Fermi* and *INTEGRAL* (e.g., Abbott et al. 2017b; Goldstein et al. 2017; Savchenko et al. 2017). Later, a kilonova AT 2017gfo was also discovered at ~ 10 h after this merger (e.g., Abbott et al. 2017b; Andreoni et al. 2017; Arcavi et al. 2017; Coulter et al. 2017). More than two different radioactive-powered components were invoked to interpret the observed AT 2017gfo light curves (e.g., Cowperthwaite et al. 2017; Perego et al. 2017; Tanaka et al. 2017; Villar et al. 2017; Tanaka et al. 2018; Kawaguchi et al. 2018; Wu et al. 2019). An afterglow source coincident with this kilonova from X-ray to radio was subsequently observed (e.g., Margutti et al. 2017; Troja et al. 2017; Dobie et al. 2018; Lyman et al. 2018; Ghirlanda et al. 2019). Neutrino observations with ANTARES, IceCube, the Pierre Auger Observatory (Albert et al. 2017), and Super-Kamiokande (Abe et al. 2018) on GW 170817 was conducted. However, no neutrinos were identified. This BNS merger and the subsequent electromagnetic counterparts further constrain the equation of the state (EoS) of NSs (e.g., Li et al. 2017, 2020).

Recently, two additional events, GW 190425 (Abbott et al. 2020a) and GW 190814 (Abbott et al. 2020b), were found to be associated with compact object mergers; at least one of the objects before mergers is in the lower mass gap, which is strange from what we currently understand as compact binary system formation channels (e.g., Safarzadeh & Loeb 2020; Zevin et al. 2020; Liu et al. 2021; Mandel et al. 2021). It is also exciting to note that two BH-NS merger events, i.e., GWs 200105 and 200115, were detected (Abbott et al. 2021). Unfortunately, neither the electromagnetic counterpart nor neutrinos were detected in these events (e.g., Dobie et al. 2019; Ackley et al. 2020; Andreoni et al. 2020; Coughlin et al. 2020; Vieira et al. 2020; Watson et al. 2020; Zhu et al. 2021).

A stellar-mass BH surrounded by a hyperaccretion disk is one of the widely accepted central engines of BNS/BH-NS mergers or massive collapsars (e.g., Liu et al. 2017a; Zhang 2018). Once the disk has a very high accretion rate, the high density and temperature of the disk cause photons to be completely trapped. Only a large number of neutrinos can escape from the disk, releasing the gravitational energy

of the BH. Annihilations of a small fraction of neutrinos can launch ultrarelativistic jets. This type of accretion disk is named a neutrino-dominated accretion flow (NDAF, e.g., Popham et al. 1999; Narayan et al. 2001; Di Matteo et al. 2002; Kohri & Mineshige 2002; Kohri et al. 2005; Lee et al. 2005; Gu et al. 2006; Chen & Beloborodov 2007; Kawanaka & Mineshige 2007; Liu et al. 2007; Kawanaka et al. 2013; Xue et al. 2013); for reviews, see Liu et al. (2017a) and Zhang (2018). Neutrino emission and GWs induced by the jet precession or anisotropic neutrinos in the NDAF model have been investigated (e.g., Suwa & Murase 2009; Romero et al. 2010; Sun et al. 2012; Liu et al. 2016, 2017b; Song et al. 2018, 2020; Wei et al. 2019; Wei & Liu 2020). Besides that, the Blandford-Znajek (BZ) mechanism (Blandford & Znajek 1977) is another way to release energy in BH hyperaccretion scenario.

The anisotropic multimessenger observation of GRBs, kilonovae, neutrinos, and GWs from NDAFs could reveal the BNS/BH-NS merger mechanism, the properties of the outflows, the dynamics of the disk, and the synthesis of the elements. The outline of this paper is as follows. In Section 2, we briefly study NDAFs with outflows. In Section 3, we investigate disk-outflow-driven (DOD) kilonovae, taking into account the anisotropic mass and velocity distributions of the outflows. In Section 4, we present the anisotropic NDAF electron antineutrino spectra by considering the general relativistic effects. In Section 5, we address isotropic GWs and their detectability. A brief summary is provided in Section 6.

2. NDAFS WITH OUTFLOWS

Disk outflows play an important role in critical accretion systems. We first introduce a well-known relation between the local accretion rate for any radius \dot{M} and the mass supply rates at the outer boundary of the disk \dot{M}_{outer} , which can be expressed by a power law form (e.g., Blandford & Begelman 1999; Yuan et al. 2012a; Yuan & Narayan 2014; Sun et al. 2019; Liu et al. 2020), i.e.,

$$\dot{M} = \dot{M}_{\text{outer}} \left(\frac{R}{R_{\text{outer}}} \right)^p, \quad (1)$$

where p is the index parameter that determines the strength of the outflows and R_{outer} is the outer boundary of the disk.

The above relation was first presented by Blandford & Begelman (1999) for advection-dominated accretion flows (ADAFs). We consider that this power-law form of the local accretion rate can also be applied to the NDAF models. The reasons are as follows. First, Liu et al. (2012a) investigated the vertical distribution of the Bernoulli parameter in NDAFs, we

found that in the outer region the Bernoulli parameter is positive, therefore, outflows might be formed in this region. Actually, many numerical simulations on NDAFs showed that the disk outflows are indispensable (e.g., Fernández & Metzger 2013; Fernández et al. 2015; Just et al. 2015; Wu et al. 2016; Lippuner et al. 2017; Siegel & Metzger 2017). Second, NDAFs are the naturally extended branch of slim disks for very high accretion rates in the well-known $\dot{M} - \Sigma$ plane (Liu et al. 2017a), where Σ and \dot{M} are the surface density of the disk and the accretion rate, respectively. Meanwhile, the outer region of NDAFs is indeed advection-dominated (e.g., Popham et al. 1999; Liu et al. 2007). Third, the efficiency of neutrino emission in the systems of Schwarzschild BHs surrounded by NDAFs without outflows is generally estimated, i.e., $L_\nu/\dot{M}c^2 \lesssim 0.035$ for $\dot{M} \lesssim 1 M_\odot \text{ s}^{-1}$ (e.g., Kawanaka & Mineshige 2007), where L_ν is the total neutrino luminosity. For the case of NDAF with outflows, the values of the above efficiency are in the range between a few percent and nearly 10% for all cases of Just et al. (2015). This result indicates that the NDAF with outflows is radiatively inefficient, which is similar to the ADAF model. The NDAF outflows are widely applied to the nucleosynthesis and dynamic motions in collapsar and merger scenarios (e.g., Surman et al. 2008, 2011; Song et al. 2018; Song & Liu 2019; Liu et al. 2019, 2020). Outflows are generated in the advection-dominated region, which leads to the low net accretion rate in the inner region, thus the neutrino-cooling-dominated region should be very narrow. Hence we roughly adopted the above power-law form to describe the outflows of the whole NDAFs.

In our calculation, the inner boundary and the outer boundary of the disk are taken as $R_{\text{inner}} = 2.3 R_g$ (for the BH mass $M_{\text{BH}} = 3 M_\odot$) and $R_{\text{outer}} = 50 R_g$, respectively, where $R_g = GM_{\text{BH}}/c^2$ is the Schwarzschild radius. The detailed dynamic equations are adopted from Liu et al. (2010) and Sun et al. (2012), from which the structure of a steady and axisymmetric NDAF can be calculated.

The total pressure P consists of four terms, namely, the gas pressure, the radiation pressure, the electron degeneracy pressure, and the neutrino pressure (e.g., Kohri et al. 2005; Liu et al. 2007), which can be written as

$$P = P_{\text{gas}} + P_{\text{rad}} + P_e + P_\nu, \quad (2)$$

and the energy balance equation is expressed as

$$Q_{\text{vis}}^+ = Q_{\text{adv}}^- + Q_{\text{photondis}}^- + Q_\nu^-, \quad (3)$$

where Q_{vis}^+ is the viscous heating rate and Q_{adv}^- , $Q_{\text{photondis}}^-$, and Q_ν^- are the advective cooling rate,

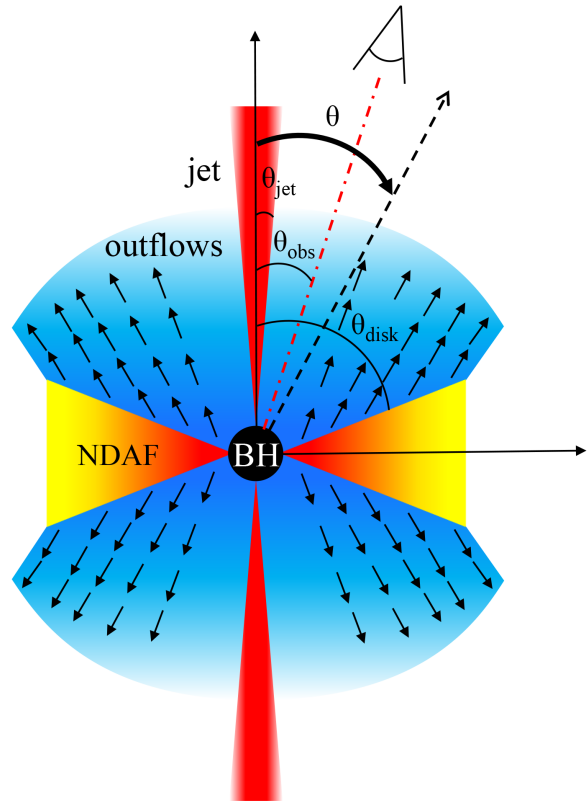


Figure 1. Schematic diagram of NDAFs with outflows.

the photodisintegration of the α -particle cooling rate, and the neutrino loss cooling rate, respectively (e.g., Kohri et al. 2005; Liu et al. 2007; Xue et al. 2013). The term $Q_{\text{photondis}}^-$ is always ignored because it only shows the little effect in a narrow middle region of the disk (e.g., Janiuk et al. 2004; Liu et al. 2007). The details of the neutrino physics related to the above equations are adopted from Liu et al. (2017a). It should be mentioned that the local net accretion rate \dot{M} is applied, so there are no terms of the local outflow pressure and cooling rate in the EoS and the energy equation. Thus, they only depend on the difference in the total pressure and viscous heating rates between two adjacent radii (Liu et al. 2020). This method is appropriate in the numerical calculations, which has been further verified by comparing the Bernoulli parameters (Liu et al. 2012a) and our primary NDAF simulations.

Liu et al. (2015) showed that in most short-duration GRB (SGRB) cases, the fallback remnant mass is less than $\sim 0.5 M_\odot$ and can reach $\sim 0.8 M_\odot$ in BH-NS merger cases (Liu et al. 2012b). The total remnant mass of BNS mergers is generally smaller than that of BH-NS mergers, which depends on the EoS of NSs, the mass ratio of the binary, the total binary mass,

and the orbital period (e.g., Oechslin & Janka 2006; Foucart 2012; Foucart et al. 2014; Dietrich et al. 2015; Just et al. 2015; Kiuchi et al. 2015). In the following, we give four typical cases, i.e., $(p, (M_{\text{disk}} + M_{\text{outflow}})/M_{\odot}) = (0.3, 0.2), (0.8, 0.2), (0.3, 0.5),$ and $(0.8, 0.5)$, where M_{disk} is the time-independent disk mass and M_{outflow} is the total net outflow mass (see Table 1). The sum of these masses represents the total fall back remnant mass around the BH. The disk mass can be constrained by $M_{\text{disk}} = 4\pi \int_{R_{\text{inner}}}^{R_{\text{outer}}} \rho R H dR$, where ρ and H are the density and half-thickness of the disk, respectively. Note that $p = 0.3$ and 0.8 represent the weak and strong disk outflows, and $M_{\text{disk}} + M_{\text{outflow}} = 0.2$ and $0.5 M_{\odot}$ denote the fall back remnant mass in the cases of BNS and BH-NS mergers, respectively. Here, we set the dimensionless BH spin parameter $a_* = 0.9$ since the post-merger BH is generally a fast rotator (e.g., Popham et al. 1999; Janiuk & Proga 2008; Liu et al. 2015; Song et al. 2015), and the viscous parameter of the disk $\alpha = 0.1$.

3. DOD KILONOVAE

3.1. Methods

The neutron-rich material ejected during compact object mergers can produce elements heavier than iron through the r -process (e.g., Lattimer & Schramm 1974; Symbalisty & Schramm 1982). Li & Paczyński (1998) first noted that the radioactive decay of these elements could feed the supernova (SN)-like thermal transient source. Metzger et al. (2010) calculated the luminosity of an optical-infrared thermal transient source from a BNS merger and named it “kilonova”. Tanaka & Hotokezaka (2013) and Barnes & Kasen (2013) showed that lanthanides have a higher opacity than iron. In addition, there are several main additional energy sources, such as the decay of free neutrons (e.g., Metzger et al. 2015) and the shock heating from the collision of relativistic jets with the ejecta (e.g., Bucciantini et al. 2012; Gottlieb et al. 2018; Piro & Kollmeier 2018). Unlike the roughly isotropic distribution of the ejecta from BNS mergers, the dynamical ejecta from BH-NS mergers predominantly distribute over the orbital plane in the shape of a crescent, with a small angle in the vertical direction and sweeping across half the plane in the horizontal disk direction (e.g., Kyutoku et al. 2013, 2015; Kawaguchi et al. 2016; Zhu et al. 2020). In addition to the ejecta from mergers, winds from a long-lived magnetar (e.g., Yu et al. 2013, 2018; Metzger & Piro 2014; Ren et al. 2019) or the outflows from an accretion disk (e.g., Just et al. 2015; Wu et al. 2016; Perego et al. 2017; Siegel & Metzger 2017; Song et al. 2018) can be considered the other significant ejecta source to power the luminous kilonova.

During the past few years, several SGRBs associated with kilonova candidates were searched, i.e., GRBs 130603B (e.g., Berger et al. 2013; Tanvir et al. 2013), 050709 (e.g., Jin et al. 2016), 060614 (e.g., Jin et al. 2015; Yang et al. 2015), and 070809 (e.g., Jin et al. 2020).

In this section, we revisit the DOD kilonova light curves in different optical bands. NDAF outflows with anisotropic mass and velocity distributions might produce anisotropic DOD kilonovae. Due to the geometry of outflows, we sum the individual contributions of materials in a solid angle $\Delta\Omega$ to compute light curves. Figure 1 shows a schematic diagram of a BH surrounded by an NDAF with outflows.

Yuan et al. (2012b, 2015) simulated the mass and velocity distributions of the outflows from the hot accretion flows with Eddington accretion rate. The difference on the accretion rates between NDAFs and hot accretion disks is about 16 orders of magnitude. Since NDAFs are similar to the radiatively inefficient ADAFs on the dynamics (e.g., Just et al. 2015), we adopt their results to build the outflow distributions from NDAFs, which are also briefly verified by our primary simulations. The mass distribution of the outflow material can be defined as

$$M(\theta) = M_0 \left(\frac{\theta}{\theta_0}\right)^k, \quad \theta_{\text{jet}} < \theta < \theta_{\text{disk}}, \quad (4)$$

where θ_{jet} and θ_{disk} are respectively the half-opening angles of the jet and the disk in the first quadrant as shown in Figure 1, and then we set $\theta_0 = \theta_{\text{jet}}$. The index $k \approx 3.72$, which is fitted from the two-dimensional simulations in Yuan et al. (2012b, 2015). Here we assume that the outflows escape from the disk independent of the radius, because their distribution is not sensitive for the far enough cases. The mass normalization is determined by

$$M_{\text{outflow}} = 2 \int_{\theta_{\text{jet}}}^{\theta_{\text{disk}}} \int_0^{2\pi} M(\theta) \sin\theta d\theta d\varphi, \quad (5)$$

from which can obtain the value of M_0 . The outflows are composed of blobs with the same velocities, so $v(\theta)$ is written as

$$v(\theta) = v_0 \left(\frac{\theta}{\theta_0}\right)^s, \quad \theta_{\text{jet}} < \theta < \theta_{\text{disk}} \quad (6)$$

with $s \approx -1.13$ and $v_0 \approx 0.47 c$. Obviously, the rangeability of the outflow velocity is much smaller than that of the outflow mass. It should be mentioned that the range of θ should exclude the jet and disk opening angles as shown in Figure 1.

The material of outflows at a certain solid angle $M(\theta)\Delta\Omega$ is divided into $N - 1$ layers with a constant expansion velocity $v(\theta)$. Here, we define the mass layers from the bottom $R_{\text{min}}(\theta) = v(\theta)t$ to the head layers

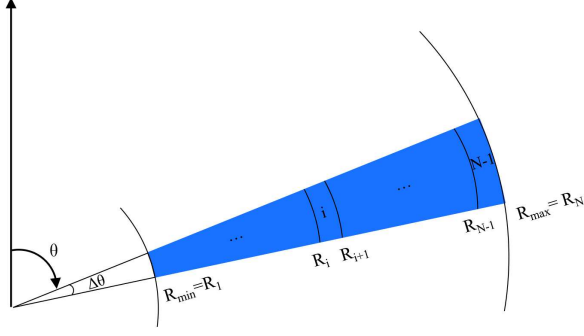


Figure 2. Schematic diagram of ejecta divided into $N - 1$ layers.

$R_{\max}(\theta) = R_0 + v(\theta)t$ by the subscript $i = 1, 2, \dots, N - 1$, where $R_0 = 10^8$ cm (much larger than the outer boundary of the disk) is the initial radius conditions of the outflows. The location of the i th layer in a solid angle at time t is $R_i(\theta)$ as shown in Figure 2.

For a matter with the same velocity at a solid angle $\Delta\Omega$, the mass of the i th layer is

$$m_i = M \frac{R_{i+1}^3 - R_i^3}{R_{\max}^3 - R_{\min}^3} \Delta\Omega. \quad (7)$$

By improving a unified kilonova model (e.g., Metzger 2019), the thermal energy E_i evolution of the i th layer at $\Delta\Omega$ is expressed as

$$\frac{dE_i}{dt} = m_i \dot{q}_r \eta_{\text{th}} - \frac{E_i}{R_i} \frac{dR_i}{dt} - L_i, \quad (8)$$

where \dot{q}_r is the radioactive energy supplied per unit mass, η_{th} is the thermal efficiency of the radioactive energy supply, and L_i is the observed luminosity contributed by this layer. The three terms on the r.h.s in order are the energy produced by the radioactive heavy element decay, the adiabatic expansion cooling, and the radiation cooling in each layer.

The radioactive energy supply per unit mass can be written as (e.g., Korobkin et al. 2012)

$$\dot{q}_r = 4 \times 10^{18} \left[\frac{1}{2} - \frac{1}{\pi} \arctan \left(\frac{t - t_0}{\sigma} \right) \right]^{1.3} \text{erg s}^{-1} \text{g}^{-1}, \quad (9)$$

where $t_0 = 1.3$ s and $\sigma = 0.11$ s. Its thermalization efficiency is expressed as (e.g., Barnes et al. 2016)

$$\eta_{\text{th}} = 0.36 \left[\exp(-0.56 t_{\text{day}}) + \frac{\ln(1 + 0.34 t_{\text{day}}^{0.74})}{0.34 t_{\text{day}}^{0.74}} \right], \quad (10)$$

where $t_{\text{day}} = t/1\text{day}$.

The observed luminosity released of the i th layer at $\Delta\Omega$ is

$$L_i = \frac{E_i}{\max[t_{d,i}, t_{lc,i}]}, \quad (11)$$

where $t_{d,i}$ is the radiation diffusion timescale of the i th layer, and $t_{lc,i} = R_i/c$ represents the light-crossing time.

The radiation diffusion timescale is described as

$$t_{d,i} = \frac{3\kappa}{\Delta\Omega R_i c} \sum_{j=i}^{N-1} m_j. \quad (12)$$

Finally, by summing the radiation luminosity contributed of all layers at $\Delta\Omega$, the total bolometric luminosity L_{bol} of outflows at $\Delta\Omega$ is given as

$$L_{\text{bol}} = \sum_{i=1}^{N-1} L_i. \quad (13)$$

Taking into account the blackbody radiation spectrum, the radiation of the ejecta is always assumed to originate from the photosphere R_{ph} and the effective temperature of each point of the DOD kilonova emission can be expressed as

$$T_{\text{eff}} = \left(\frac{L_{\text{bol}}}{\sigma_{\text{SB}} \Delta\Omega R_{\text{ph}}^2} \right)^{1/4}, \quad (14)$$

where σ_{SB} is the Stephan-Boltzmann constant and the photosphere radius R_{ph} is defined as that of the mass layer beyond which the optical depth equals unity. The ejecta is only distributed between R_{\min} and R_{\max} , so we have to adopt such an approximate method that if the total optical depth of the ejecta $\tau_{\text{tot}} \leq 1$, the photosphere radius R_{ph} is the minimum radius R_{\min} (e.g., Yu et al. 2018; Ren et al. 2019); if the optical depth of the $(N - 1)$ th layer $\tau_{N-1} > 1$, $R_{\text{ph}} = R_{\max}$.

The total optical depth is $\tau_{\text{tot}} = \sum_{i=1}^{N-1} \tau_i$, τ_i is the optical depth of the i th layer and can be described as $\tau_i = \int_{R_i}^{R_{i+1}} \kappa \rho_{\text{outflow}} dR$, where ρ_{outflow} is the outflow density and can be derived from the outflow distribution. The value of the average effective gray opacity $\kappa \sim 0.5 - 30 \text{ cm}^2 \text{ g}^{-1}$ represents a wide range from lanthanum-free to lanthanum-rich matter (e.g., Tanaka et al. 2020). Here, $\kappa = 20 \text{ cm}^2 \text{ g}^{-1}$ is adopted.

Subject to the propagation of light, the photons are emitted at a given time t and reach the observer at time

$$t_{\text{obs}} = t + \frac{[R_{\text{ph}}(\theta_{\text{obs}}) - R_{\text{ph}}(\theta)] \cos \Delta\theta}{c}, \quad (15)$$

where $\Delta\theta$ is the angle between the direction of movement of the point on the photosphere layer and the direction of the line of sight.

The distribution of the observed flux with the solid angle is

$$dF_\nu(\nu, t_{\text{obs}}) = \frac{2\pi h\nu^3}{c^2} \frac{1}{1 - \exp(h\nu/k_{\text{B}}T_{\text{eff}})} \frac{R_{\text{ph}}^2 d\Omega}{4\pi D_L^2}, \quad (16)$$

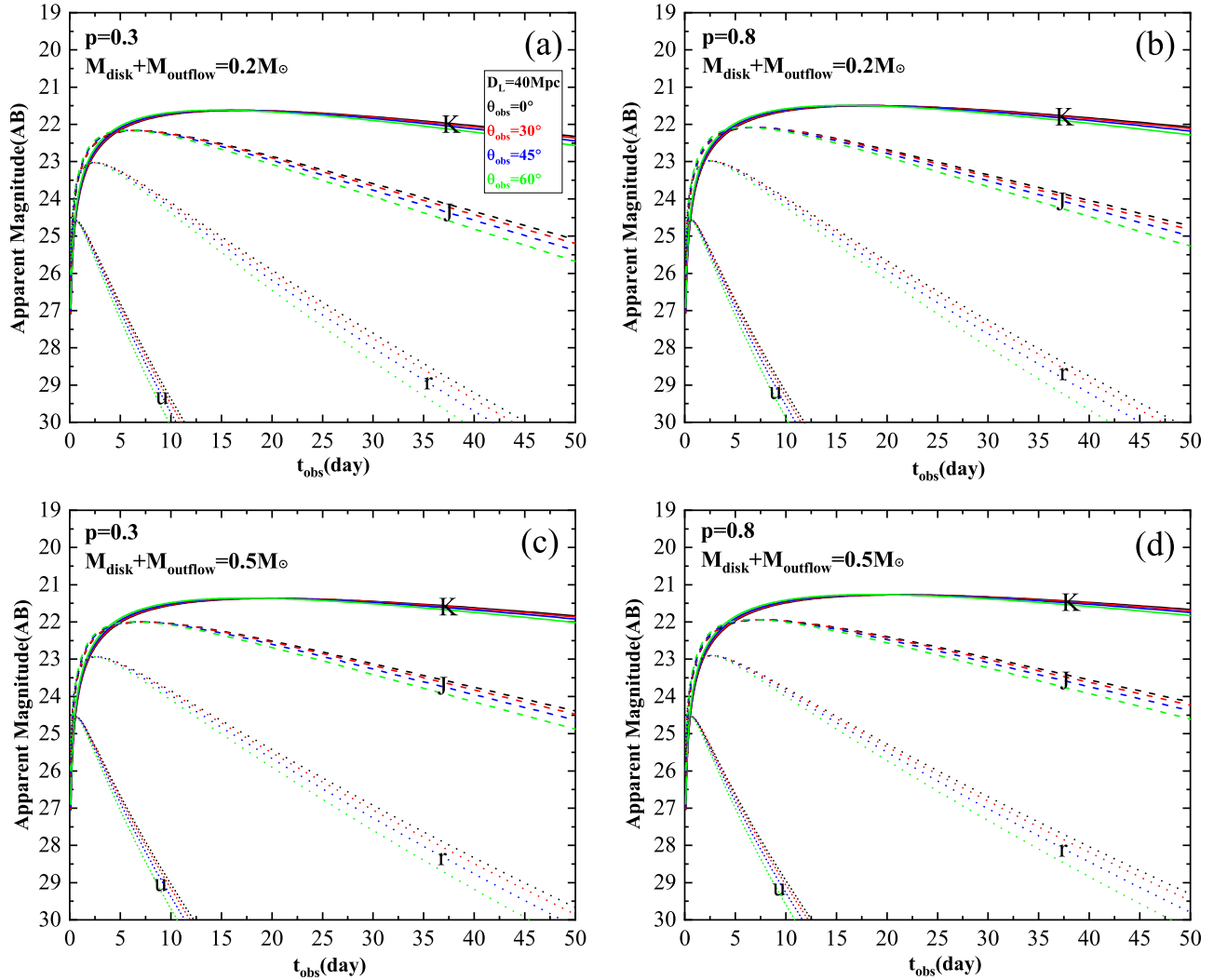


Figure 3. Viewing-angle-dependent urJK-band light curves of DOD kilonovae at a distance of 40 Mpc for the cases of $(p, (M_{\text{disk}} + M_{\text{outflow}})/M_{\odot}) = (0.3, 0.2), (0.8, 0.2), (0.3, 0.5),$ and $(0.8, 0.5)$. The black, red, blue, and green lines denote the viewing angles $\theta_{\text{obs}} = 0^{\circ}, 30^{\circ}, 45^{\circ},$ and 60° , respectively. The solid, dashed, thin dotted, and thick dotted lines represent the K, J, r, and u bands, respectively.

where k_{B} is the Boltzmann constant, h is the Planck constant, and D_{L} is the luminosity distance.

According to the half-day arc equation, i.e.,

$$\varphi(\theta) = \arccos(-\cot\theta\cot\theta_{\text{obs}}), \quad (17)$$

the range of longitude visible to the observer in a certain θ is $[-\varphi(\theta), \varphi(\theta)]$ if the observer is located at $\varphi = 0^{\circ}$.

The observed flux density of the DOD kilonova emission from a certain viewing angle θ_{obs} in the first quadrant can be written as

$$F_{\nu}(\nu, t_{\text{obs}}) = 2 \int_{\theta_{\text{jet}}}^{\theta_{\text{obs}} + \frac{\pi}{2}} \int_0^{\varphi(\theta)} dF_{\nu}. \quad (18)$$

In our calculation, we set $\theta_{\text{jet}} = 5^{\circ}$, which corresponds to the typical value of the half-opening angles

of jets; $\theta_{\text{disk}} = 80^{\circ}$, which is adopted from the typical half-opening angle of the inner region of NDAFs (e.g., Popham et al. 1999; Liu et al. 2007), and taken into account that the outflows far away from the disk might diffuse in the θ -direction; and $D_{\text{L}} = 40$ Mpc. Finally, we can express the monochromatic AB magnitude M_{ν} by the relation of $M_{\nu} = -2.5\log_{10}(F_{\nu}/3631\text{Jy})$.

3.2. Results

Figure 3 shows the viewing-angle-dependent urJK-band light curves of DOD kilonovae at a distance of 40 Mpc. The black, red, blue, and green lines denote the viewing angles $\theta_{\text{obs}} = 0^{\circ}, 30^{\circ}, 45^{\circ},$ and 60° , respectively. The solid, dashed, thin dotted, and thick dotted lines represent the K, J, r, and u bands, respectively. One can find that the DOD kilonova luminos-

ity decreases as the viewing angle θ_{obs} increases. These properties appear in the J, u, and r bands but in the K band. This is because the flux at different solid angles is related to the position of the photosphere radius. The minimum (or maximum) values of the outflow mass (or velocity) appear near the pole direction. Thus the results show that the anisotropy is not very sensitive to the mass distribution and mainly determined by the velocity distributions.

As comparisons among four figures, the values of p and $M_{\text{disk}} + M_{\text{outflow}}$ have little effects on the luminosities for a certain viewing angle. In other words, there is slight difference on the light curves in both the BNS and BH-NS merger cases, which is caused by the value of the outflow velocity rather than that of the outflow mass. The typical magnitudes are dimmer than ~ 24 mag in the ultraviolet band and dimmer than ~ 21 mag in the infrared band. The emission peaks appear at ~ 1 day in the u-band and ~ 1 week in the K-band. The DOD kilonova emission is dominated by the K-band after ~ 5 days. The mean power injected by the r -process in the total outflows can be obtained by $\bar{P}_r = \int_0^{50 \text{ days}} M_{\text{outflow}} \dot{q}_r \eta_{\text{th}} dt / (50 \text{ days})$, and the mean bolometric luminosity of the total outflows is calculated by $\bar{L}_{\text{bol}} = \int_0^{50 \text{ days}} \int_0^{4\pi} L_{\text{bol}} d\Omega dt / (50 \text{ days})$, which are shown in Table 1. We find that the typical DOD kilonovae are dimmer than AT 2017gfo associated with BNS mergers. Since the distributions of the outflow mass and velocity are inversely correlated with θ , it is difficult for the DOD kilonovae to be dominant in AT 2017gfo. This is consistent with previous kilonova models where AT 2017gfo is composed of different components and mainly powered by the dynamical ejecta (e.g., Cowperthwaite et al. 2017; Kasen et al. 2017; Villar et al. 2017). For the case of BH-NS mergers, the dynamical ejecta are mainly on the orbital plane, so the role of NDAF outflows should be more pronounced and they might become the dominant components. In other words, the DOD kilonovae might be unobservable in the BNS mergers, but can be detected in the BH-NS mergers occurred in the nearby universe. If a DOD kilonova is associated with GW 200105 at a distance of ~ 300 Mpc, their K-band peak luminosities at AB magnitudes are less than 26 mag; thus, they are too faint to be detected by the telescopes performing the observation tasks on GW electromagnetic counterparts. Moreover, the DOD kilonova has at least a natural blue and red component due to the anisotropic outflow mass and velocity distribution from the pole to equator directions.

Unlike the roughly isotropic distribution of the ejecta from BNS mergers, the dynamical ejecta from BH-NS mergers predominantly distribute over the orbital plane

in the shape of a crescent, with a small angle in the vertical direction and sweeping across half the plane in the horizontal disk direction

Neutrino irradiation may increase the electron fraction Y_e of neutron-rich material (particularly $\nu_e + n \rightarrow p + e^-$, e.g., Korobkin et al. 2012; Wanajo et al. 2014; Kyutoku & Kashiyaama 2018). We reasonably ignore this effect because the outflows are mainly launched from the outer region of the disk, where only a small number of neutrinos are produced, and the neutrino optical depth of the disk outflows is generally thin. From the distributions of the outflow density and temperature, we can estimate the sum of absorptive and scattering optical depths of neutrinos (e.g., Di Matteo et al. 2002; Gu et al. 2006) escaped along the vertical direction at $30 R_g$, $\sim 2 \times 10^{-8}$.

4. MEV NEUTRINOS

4.1. Methods

MeV neutrinos from core-collapse SNe (CCSNe, e.g., Friedland 2010; Warren et al. 2020) and their central NDAFs (e.g., Liu et al. 2016; Wei et al. 2019; Song et al. 2020) have been investigated. Although the neutrino luminosity of NDAFs is 1 – 3 orders of magnitude lower than that of CCSNe, a certain number of neutrinos could still be detected in the Local Group by prospective detectors (e.g., Liu et al. 2016). In this work, the anisotropic neutrino emission from NDAFs in binary compact object mergers is calculated.

We employ ray-tracing methods (e.g., Fanton et al. 1997; Li et al. 2005) to account for the propagation of neutrinos and calculate the observed neutrino energy spectrum, which is primarily influenced by the general relativity under the strong gravity of the central BH. Here, we assume that the equatorial plane is the location of the main source of neutrinos, the neutrinos are emitted isotropically from all radii of the disk, and the disk thickness is neglected.

The neutrino trajectories from the emitter must satisfy the geodesic equation (Carter 1968). Therefore, the location of the launch point of the disk can be tracked by each pixel point of the observed image. The neutrino energy redshift can be calculated by integrating the velocity and gravitational potential at the corresponding emission position point. The observed neutrino flux is obtained by integration of all pixel points (e.g., Liu et al. 2016; Wei et al. 2019), i.e.,

$$F_{E_{\text{obs}}} = \int_{\text{image}} g^3 I_{E_{\text{em}}} d\Omega_{\text{obs}}, \quad (19)$$

where $g \equiv E_{\text{obs}}/E_{\text{em}}$ is the energy shift factor, E_{em} is the neutrino emission energy from the local disk, E_{obs} is

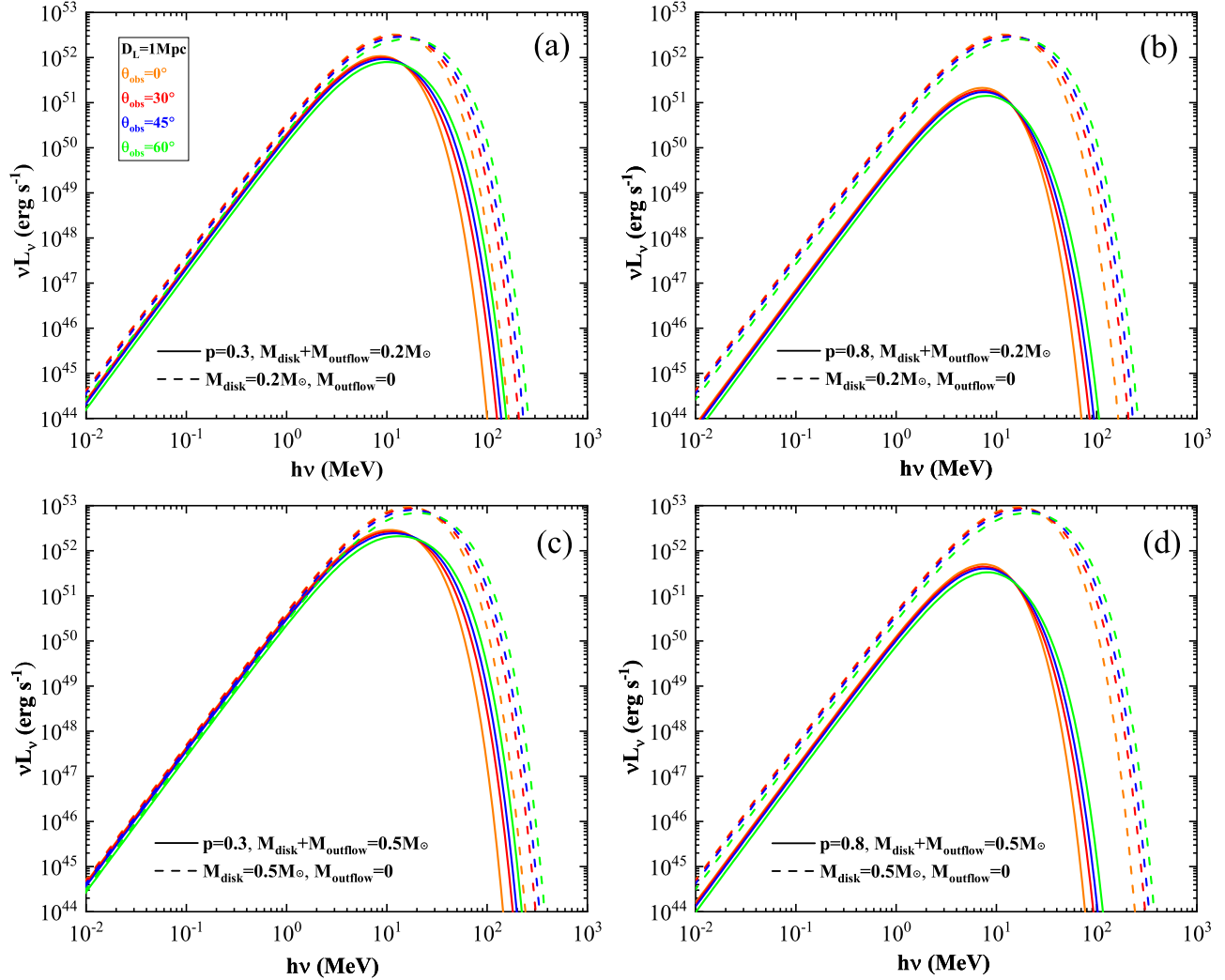


Figure 4. Viewing-angle-dependent electron antineutrino spectra of NDAFs with (solid lines) or without (dashed lines) outflows in merger scenarios at a distance of 1 Mpc. The orange, red, blue, and green lines correspond to $\theta_{\text{obs}} = 0^\circ, 30^\circ, 45^\circ,$ and 60° , respectively.

the observed neutrino energy, and Ω_{obs} is the solid angle of the disk image with respect to the observer. Based on the cooling rate via electron antineutrinos $Q_{\bar{\nu}_e}$, the local emissivity $I_{E_{\text{em}}}$ is obtained by

$$I_{E_{\text{em}}} = Q_{\bar{\nu}_e} \frac{F_{E_{\text{em}}}}{\int F_{E_{\text{em}}} dE_{\text{em}}}, \quad (20)$$

where $F_{E_{\text{em}}} = E_{\text{em}}^2 / [\exp(E_{\text{em}}/kT - \eta) + 1]$ is the unnormalized Fermi-Dirac spectrum (e.g., Rauch & Blandford 1994; Fanton et al. 1997; Li et al. 2005; Liu et al. 2016). Therefore, the luminosity distribution can be derived as

$$L_\nu = 4\pi D_L^2 F_{E_{\text{obs}}}. \quad (21)$$

It should be mentioned that electron antineutrinos can be detected via the inverse beta decay (IBD) reaction, and the IBD is the best channel for the most of present

and upcoming neutrino detectors. Thus we discuss the electron antineutrino spectra here.

4.2. Results

Figure 4 shows the effects of the viewing angles on the electron antineutrino spectra of NDAFs with different outflow strengths (solid lines) and without outflows (dashed lines) in the BNS/BH-NS merger scenarios at a distance of 1 Mpc. The orange, red, blue, and green lines correspond to the viewing angles $\theta_{\text{obs}} = 0^\circ, 30^\circ, 45^\circ,$ and 60° , respectively. In the case of NDAFs with different outflow strengths, the neutrino energies are generally in the range of $\sim 10 \text{ keV} - 100 \text{ MeV}$, and the peaks are at approximately $10 - 20 \text{ MeV}$. The corresponding neutrino luminosities of NDAFs reach $\sim 2 \times 10^{51} - 3 \times 10^{52} \text{ erg s}^{-1}$. However, in the case of NDAFs without outflows, the peaks of neutrino energies move slightly to the higher

values, and the maximum neutrino luminosity can be $\sim 3 \times 10^{52} - 9 \times 10^{52} \text{ erg s}^{-1}$. Moreover, we find that the high-energy ($\gtrsim 10 \text{ MeV}$) neutrinos have a more anisotropic luminosity, but the low-energy ($\lesssim 10 \text{ MeV}$) neutrinos are approximately isotropic. High-energy neutrinos are mainly produced in the inner region of the disk, which means that they are significantly deflected to a large viewing angle by BH gravity. Therefore, the high-energy neutrino luminosities increase with increasing viewing angles. In contrast, low-energy neutrinos are mainly generated in the outer region of the disk, so the general relativity has weak effects on them. Comparing the weak and strong outflows of NDAFs in BNS or BH-NS merger cases, we find that the neutrino luminosity decreases with increasing outflow strength. Actually, there is a natural competition between the masses and energies of the outflows and inflows (e.g., Song et al. 2018; Liu et al. 2020).

The effects of neutrino oscillations are not taken into account, which not only corrects the neutrino energy spectra but also decreases the detectable neutrino fluxes by a factor of up to $\sim 2 - 3$ (e.g., Friedland 2010; Duan & Friedland 2011; Cherry et al. 2012; Liu et al. 2016). Kyutoku & Kashiyama (2018) proposed that monitoring $\gtrsim 2500$ merger events within $\lesssim 200 \text{ Mpc}$ identified by GW detectors could give us a chance of detecting a single neutrino for the merger rate of $1 \text{ Mpc}^{-3} \text{ Myr}^{-1}$ with a human time-scale operation of $\sim 80 \text{ Myr}$. MeV neutrinos have not been detected in any of the recent binary compact object mergers, probably because they are too far away to be detected. The detectable neutrinos from NDAFs in merger events also need strict requirements on the distance (or the brightness), which is at least similar to the possibly detectable distance of NDAFs in the center of CCSNe, $\lesssim 1 \text{ Mpc}$, i.e., location in the Local Group (see e.g., Liu et al. 2016). Moreover, as mentioned in the above section, we ignore the interaction between neutrinos escaped from the disk and the high-velocity disk outflows.

5. GWS

5.1. Methods

Epstein (1978) first proposed GW radiation resulting from anisotropic neutrinos, and the methods have been applied to CCSNe (e.g., Burrows & Hayes 1996; Kotake et al. 2006, 2007). GWs arising from anisotropic neutrino emission in NDAFs have been investigated (e.g., Suwa & Murase 2009; Kotake et al. 2012; Liu et al. 2017b; Song et al. 2020; Wei & Liu 2020). Liu et al. (2017b) examined the BH spin and accretion rate impacts on the strains of GWs in NDAFs; compared their strains, frequencies, and detection possi-

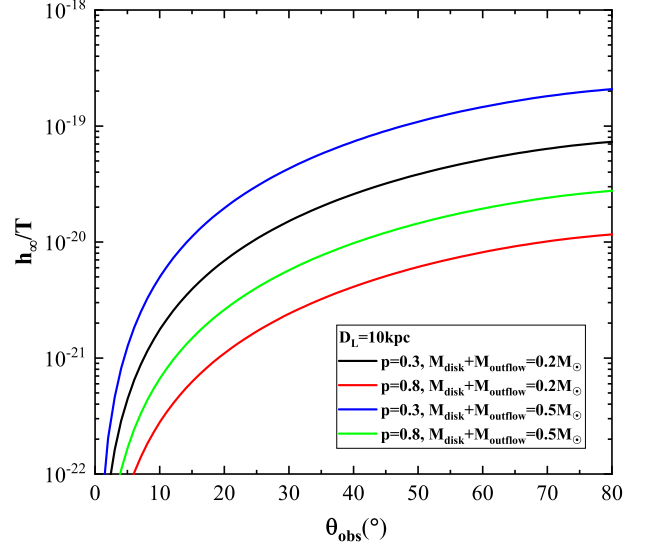


Figure 5. h_∞/T as a function of the viewing angle θ_{obs} at a distance of 10 kpc for four cases.

bility to those from magnetars; and presented no GW emission from the BZ mechanism (Blandford & Znajek 1977). The above works mainly focus on the collapsar scenario, here we adopt the similar method to calculate the GWs from NDAFs in BNS/BH-NS merger scenarios.

For long-lived neutrino emissions, the GW amplitude converges to a nonvanishing value h_∞ . It is related to the viewing angle θ_{obs} and is derived as follows (e.g., Suwa & Murase 2009):

$$h_\infty(\theta_{\text{obs}}) = \frac{2G(1 + 2 \cos \theta_{\text{obs}})}{3c^4 D_L} \tan^2 \left(\frac{\theta_{\text{obs}}}{2} \right) \bar{L}_\nu T, \quad (22)$$

where $\bar{L}_\nu = 2\pi \int_0^T \int_{R_{\text{inner}}}^{R_{\text{outer}}} Q_\nu^- R dR dt / T$ and T are the mean neutrino luminosity above (or below) the disk (see Table 1) and the center engine activity duration, respectively.

Considering an SGRB powered by an NDAF as one single pulse, we construct the luminosity of neutrino evolution of time $L_\nu(t)$ as (e.g., Suwa & Murase 2009)

$$L_\nu(t) = \bar{L}_\nu \Theta(t) \Theta(T - t), \quad (23)$$

where Θ is the Heaviside step function. Central engine intermittent activity should also be considered. This motivates us to list the case of multiple pulses,

$$L_\nu(t) = \sum_{i=1}^{N'} \frac{\bar{L}_\nu T}{N' \delta t} \Theta \left(t - \frac{i}{N'} T \right) \Theta \left(\frac{i}{N'} T + \delta t - t \right), \quad (24)$$

where N' is the number of pulses and δt is the duration of one pulse. $N' \delta t$ should be shorter than T , except in the case of a single pulse of $N' = 1$.

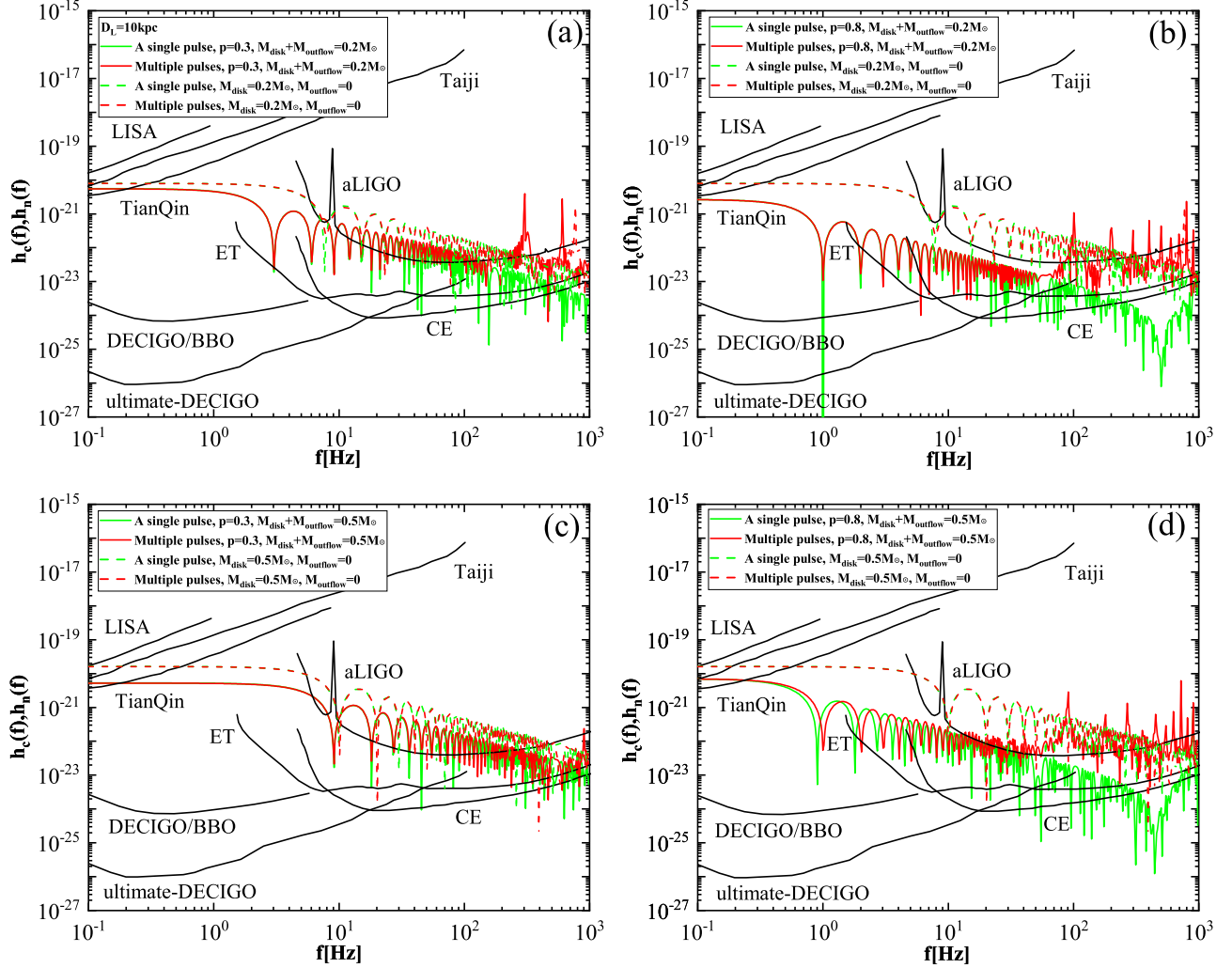


Figure 6. Characteristic strains of GWs from NDAFs with (solid lines) or without (dashed lines) outflows in BNS/BH-NS merger scenarios at a distance of 10 kpc. The green and red lines represent the cases of SGRBs with a single pulse and the multiple pulses, respectively. The black solid lines represent the sensitivity lines (the noise amplitudes h_n) of aLIGO, ET, CE, LISA, Taiji, TianQin, DECIGO/BBO, and ultimate-DECIGO.

$L_\nu(t)$ is expressed as an inverse Fourier transform into the form,

$$L_\nu(t) = \int_{-\infty}^{+\infty} \tilde{L}_\nu(f) e^{-2\pi i f t} df, \quad (25)$$

for a given frequency f .

The nonvanishing GW amplitude of NDAFs $h_+(t)$ is given by (see e.g., Müller & Janka 1997)

$$h_+(t) = \frac{2G}{3D_L c^4} \int_{-\infty}^{t-D_L/c} L_\nu(t') dt', \quad (26)$$

and the local energy flux of GWs can be estimated by (e.g., Suwa & Murase 2009)

$$\frac{dE_{\text{GW}}}{D_L^2 d\Omega dt} = \frac{c^3}{16\pi G} \left| \frac{d}{dt} h_+(t) \right|^2. \quad (27)$$

The total GW energy can be calculated by

$$E_{\text{GW}} = \frac{\beta G}{9c^5} \int_{-\infty}^{\infty} L_\nu(t)^2 dt \quad (28)$$

with $\beta \sim 0.47039$.

The GW energy spectrum can be described by

$$\frac{dE_{\text{GW}}(f)}{df} = \frac{2\beta G}{9c^5} |\tilde{L}_\nu(f)|^2. \quad (29)$$

To determine the GW detectability of NDAFs, the characteristic strain of GWs is written as (e.g., Flanagan & Hughes 1998)

$$h_c(f) = \sqrt{\frac{2}{\pi^2} \frac{G}{c^3} \frac{1}{D_L^2} \frac{dE_{\text{GW}}(f)}{df}}. \quad (30)$$

After we obtained the correlation between $h_c(f)$ and f for a single pulse and multiple pulses from SGRBs, we

Table 1. Key properties of multimessenger signals.

Luminosity (or power)	Case I	Case II	Case III	Case IV
$M_{\text{outflow}}/M_{\odot}$	0.12	0.19	0.31	0.44
$\bar{P}_r/10^{44} \text{ erg s}^{-1}$	0.46	0.72	1.15	1.67
$\bar{L}_{\text{bol}}/10^{39} \text{ erg s}^{-1}$	4.93	5.77	6.76	7.56
$\bar{L}_{\nu}/10^{53} \text{ erg s}^{-1}$	0.43	0.07	1.23	0.16
$\bar{P}_{\text{GW}}/10^{45} \text{ erg s}^{-1}$	0.88	0.07	2.38	0.43

Notes: Cases I-IV denote $(p, (M_{\text{disk}} + M_{\text{outflow}})/M_{\odot}) = (0.3, 0.2), (0.8, 0.2), (0.3, 0.5),$ and $(0.8, 0.5),$ respectively. M_{outflow} is the mass of disk outflows, and $\bar{P}_r, \bar{L}_{\text{bol}}, \bar{L}_{\nu},$ and \bar{P}_{GW} are the mean power injected by the r -process in the total outflows, the mean bolometric luminosity of the total outflows, the mean neutrino luminosity above (or below) the disk, and the mean GW power, respectively.

presented the signal-to-noise ratios (S/Ns) of the corresponding filter for GWs. The optimal S/N is

$$S/N^2 = \int_0^{\infty} d(\ln f) \frac{h_c(f)^2}{h_n(f)^2}, \quad (31)$$

where $h_n(f) = [5fS_n(f)]^{1/2}$ is the noise amplitude and $S_n(f)$ is the spectral density of strain noise when the frequency of the detector is f .

5.2. Results

Figure 5 shows h_{∞}/T as a function of the viewing angle θ_{obs} at a distance of 10 kpc. It should be noted that there is almost no GW emission in the polar direction, whereas the GW amplitudes increase with increasing viewing angle.

Figure 6 shows the characteristic strains of GWs from NDAFs with different outflow strengths in BNS/BH-NS merger scenarios at a distance of 10 kpc for four cases of SGRBs with a single pulse (green solid lines in four figures, $T = 0.3, 1, 0.1,$ and 1 s, respectively) and the multiple pulses (red solid lines in four figures, $N' = 100,$ $\delta t = 0.001$ s, and $T = 0.3, 1, 0.1,$ and 1 s, respectively). Moreover, for the cases of NDAFs without outflows, the green and red dashed lines represent the cases of SGRBs with a single pulse ($T = 0.1$ s) and the multiple pulses ($N' = 100,$ $\delta t = 0.001$ s, and $T = 0.1$ s), respectively. The durations are determined by the accretion timescales. The black solid lines represent the sensitivity curves (the noise amplitudes h_n) of the following detectors, i.e., aLIGO, ET, CE, LISA, Taiji, TianQin, DECIGO/BBO, and ultimate-DECIGO.

We can notice that the typical GW frequencies are in the ranges of $\sim 1 - 1000$ and $\sim 10 - 1000$ Hz for the cases of NDAFs with and without outflows, respectively, which is determined by the GRB variabilities ($f \sim 1/2\delta t$, see e.g., Liu et al. 2017b). The GW waveforms induced by a single pulse and the multiple pulses

are very different also caused by the distinction on the variabilities of the neutrino emission. The GW strains increase with decreasing outflow strengths, which corresponds increasing neutrino luminosities. Therefore, the GW strains reach the largest values when the NDAFs has no outflows. The mean GW power, $\bar{P}_{\text{GW}} = E_{\text{GW}}/T,$ is shown in Table 1 for four cases. Indeed, the GW emission from NDAFs is originated from the anisotropic neutrino emission. One can note that GWs from NDAFs with and without outflows can be detected by ET, CE, DECIGO/BBO, and ultimate-DECIGO in the detectable frequency of $\sim 1 - 200$ Hz and $\sim 10 - 200$ Hz at 10 kpc for SGRBs with a single pulse or the multiple pulses, respectively. The properties of this GWs are similar to those of GWs originated from a precessing jet launched by a warped NDAF (e.g., Sun et al. 2012; Liu et al. 2017b).

6. SUMMARY

In a multimessenger study of BNS/BH-NS mergers, observed signals such as GRBs, kilonova, neutrinos, and GWs can be utilized to investigate the physics of BNS/BH-NS mergers. These multimessenger signals might mingle or even be dominated by the contributions of BH-NDAF systems. In this paper, we modeled NDAFs with outflows to study anisotropic DOD kilonovae, MeV neutrinos, and GWs in BNS/BH-NS merger scenarios. For DOD kilonovae, we find that the mass distributions do not significantly affect the anisotropy of the kilonova luminosity, but the velocity distribution influences the location of the radius of the photosphere, which in turn affects the luminosity. The anisotropy of DOD kilonovae appears in the J, u, and r bands but not in the K band. Then, we study the electron antineutrino energy spectra from NDAFs with and without outflows for different viewing angles. The general relativity has an important influence on the high-energy ($\gtrsim 10$ MeV) neutrinos fluxes leading to anisotropy, but low-energy

($\lesssim 10$ MeV) neutrinos fluxes are almost isotropic. MeV neutrinos from NDAFs in the Local Group might be detectable. Furthermore, we present the GW emission arising from anisotropic neutrino radiation from merger NDAFs with and without outflows. The GW strains are totally determined by the neutrino luminosities, and they increase with increasing viewing angles. The GW signals from NDAFs with outflows could be detected within the frequency of 1–200 Hz at a distance of 10 kpc by ET, CE, DECIGO/BBO, and ultimate-DECIGO.

As shown in Figures 3 and 4, it is difficult to constrain the viewing angles just according to the individual observations of the DOD kilonovae or MeV neutrinos, but the GW detections of the merger events can

provide the morphology information of the mergers and the following BH hyperaccretion. Future joint multimessenger observations could provide effective insights into the central BH-NDAF systems created by BNS/BH-NS mergers at least in the Local Group and can be used to determine the nature of BH hyperaccretion models.

ACKNOWLEDGMENTS

We thank Da-Bin Lin, Jin-Ping Zhu, Jun-Hui Liu, Jia Ren, and Zhen-Yu Zhu for helpful discussions. This work was supported by the National Natural Science Foundation of China under grants 11822304, 12173031, and 11773053.

REFERENCES

- Abadie, J., Abbott, B. P., Abbott, R., et al. 2010, *Classical and Quantum Gravity*, 27, 173001.
doi:10.1088/0264-9381/27/17/173001
- Abbott, B. P., Abbott, R., Abbott, T. D., et al. 2017a, *PhRvL*, 119, 161101.
doi:10.1103/PhysRevLett.119.161101
- Abbott, B. P., Abbott, R., Abbott, T. D., et al. 2017b, *ApJL*, 848, L12. doi:10.3847/2041-8213/aa91c9
- Abbott, B. P., Abbott, R., Abbott, T. D., et al. 2020a, *ApJL*, 892, L3. doi:10.3847/2041-8213/ab75f5
- Abbott, R., Abbott, T. D., Abraham, S., et al. 2020b, *ApJL*, 896, L44. doi:10.3847/2041-8213/ab960f
- Abbott, R., Abbott, T. D., Abraham, S., et al. 2021, *ApJL*, 915, L5. doi:10.3847/2041-8213/ac082e
- Abe, K., Bronner, C., Hayato, Y., et al. 2018, *ApJL*, 857, L4. doi:10.3847/2041-8213/aabaca
- Ackley, K., Amati, L., Barbieri, C., et al. 2020, *A&A*, 643, A113. doi:10.1051/0004-6361/202037669
- Albert, A., André, M., Anghinolfi, M., et al. 2017, *ApJL*, 850, L35. doi:10.3847/2041-8213/aa9aed
- Andreoni, I., Ackley, K., Cooke, J., et al. 2017, *PASA*, 34, e069. doi:10.1017/pasa.2017.65
- Andreoni, I., Goldstein, D. A., Kasliwal, M. M., et al. 2020, *ApJ*, 890, 131. doi:10.3847/1538-4357/ab6a1b
- Arcavi, I., Hosseinzadeh, G., Howell, D. A., et al. 2017, *Nature*, 551, 64. doi:10.1038/nature24291
- Baiotti, L. & Rezzolla, L. 2017, *Reports on Progress in Physics*, 80, 096901. doi:10.1088/1361-6633/aa67bb
- Barnes, J. & Kasen, D. 2013, *ApJ*, 775, 18.
doi:10.1088/0004-637X/775/1/18
- Barnes, J., Kasen, D., Wu, M.-R., et al. 2016, *ApJ*, 829, 110. doi:10.3847/0004-637X/829/2/110
- Berger, E. 2014, *ARA&A*, 52, 43.
doi:10.1146/annurev-astro-081913-035926
- Berger, E., Fong, W., & Chornock, R. 2013, *ApJL*, 774, L23. doi:10.1088/2041-8205/774/2/L23
- Berger, E., Price, P. A., Cenko, S. B., et al. 2005, *Nature*, 438, 988. doi:10.1038/nature04238
- Blandford, R. D. & Begelman, M. C. 1999, *MNRAS*, 303, L1. doi:10.1046/j.1365-8711.1999.02358.x
- Blandford, R. D. & Znajek, R. L. 1977, *MNRAS*, 179, 433. doi:10.1093/mnras/179.3.433
- Bucciantini, N., Metzger, B. D., Thompson, T. A., et al. 2012, *MNRAS*, 419, 1537.
doi:10.1111/j.1365-2966.2011.19810.x
- Burrows, A. & Hayes, J. 1996, *PhRvL*, 76, 352.
doi:10.1103/PhysRevLett.76.352
- Carter, B. 1968, *Physical Review*, 174, 1559.
doi:10.1103/PhysRev.174.1559
- Chen, W.-X. & Beloborodov, A. M. 2007, *ApJ*, 657, 383.
doi:10.1086/508923
- Cherry, J. F., Wu, M.-R., Carlson, J., et al. 2012, *PhRvD*, 85, 125010. doi:10.1103/PhysRevD.85.125010
- Coughlin, M. W., Dietrich, T., Antier, S., et al. 2020, *MNRAS*, 492, 863. doi:10.1093/mnras/stz3457
- Coulter, D. A., Foley, R. J., Kilpatrick, C. D., et al. 2017, *Science*, 358, 1556. doi:10.1126/science.aap9811
- Cowan, J. J., Sneden, C., Lawler, J. E., et al. 2021, *Reviews of Modern Physics*, 93, 015002.
doi:10.1103/RevModPhys.93.015002
- Cowperthwaite, P. S., Berger, E., Villar, V. A., et al. 2017, *ApJL*, 848, L17. doi:10.3847/2041-8213/aa8fc7
- Cutler, C. & Flanagan, É. E. 1994, *PhRvD*, 49, 2658.
doi:10.1103/PhysRevD.49.2658

- Dai, Z. G., Wang, X. Y., Wu, X. F., et al. 2006, *Science*, 311, 1127. doi:10.1126/science.1123606
- Di Matteo, T., Perna, R., & Narayan, R. 2002, *ApJ*, 579, 706. doi:10.1086/342832
- Dietrich, T., Bernuzzi, S., Ujevic, M., et al. 2015, *PhRvD*, 91, 124041. doi:10.1103/PhysRevD.91.124041
- Dobie, D., Kaplan, D. L., Murphy, T., et al. 2018, *ApJL*, 858, L15. doi:10.3847/2041-8213/aac105
- Dobie, D., Stewart, A., Murphy, T., et al. 2019, *ApJL*, 887, L13. doi:10.3847/2041-8213/ab59db
- Duan, H. & Friedland, A. 2011, *PhRvL*, 106, 091101. doi:10.1103/PhysRevLett.106.091101
- Duncan, R. C. & Thompson, C. 1992, *ApJL*, 392, L9. doi:10.1086/186413
- Eichler, D., Livio, M., Piran, T., et al. 1989, *Nature*, 340, 126. doi:10.1038/340126a0
- Epstein, R. 1978, *ApJ*, 223, 1037. doi:10.1086/156337
- Fanton, C., Calvani, M., de Felice, F., et al. 1997, *PASJ*, 49, 159. doi:10.1093/pasj/49.2.159
- Fernández, R., Kasen, D., Metzger, B. D., et al. 2015, *MNRAS*, 446, 750. doi:10.1093/mnras/stu2112
- Fernández, R. & Metzger, B. D. 2013, *MNRAS*, 435, 502. doi:10.1093/mnras/stt1312
- Flanagan, É. É. & Hughes, S. A. 1998, *PhRvD*, 57, 4535. doi:10.1103/PhysRevD.57.4535
- Foucart, F. 2012, *PhRvD*, 86, 124007. doi:10.1103/PhysRevD.86.124007
- Foucart, F., Deaton, M. B., Duez, M. D., et al. 2014, *PhRvD*, 90, 024026. doi:10.1103/PhysRevD.90.024026
- Friedland, A. 2010, *PhRvL*, 104, 191102. doi:10.1103/PhysRevLett.104.191102
- Ghirlanda, G., Salafia, O. S., Paragi, Z., et al. 2019, *Science*, 363, 968. doi:10.1126/science.aau8815
- Goldstein, A., Veres, P., Burns, E., et al. 2017, *ApJL*, 848, L14. doi:10.3847/2041-8213/aa8f41
- Gottlieb, O., Nakar, E., Piran, T., et al. 2018, *MNRAS*, 479, 588. doi:10.1093/mnras/sty1462
- Gu, W.-M., Liu, T., & Lu, J.-F. 2006, *ApJL*, 643, L87. doi:10.1086/505140
- Janiuk, A., Perna, R., Di Matteo, T., et al. 2004, *MNRAS*, 355, 950. doi:10.1111/j.1365-2966.2004.08377.x
- Janiuk, A. & Proga, D. 2008, *ApJ*, 675, 519. doi:10.1086/526511
- Jin, Z.-P., Covino, S., Liao, N.-H., et al. 2020, *Nature Astronomy*, 4, 77. doi:10.1038/s41550-019-0892-y
- Jin, Z.-P., Hotokezaka, K., Li, X., et al. 2016, *Nature Communications*, 7, 12898. doi:10.1038/ncomms12898
- Jin, Z.-P., Li, X., Cano, Z., et al. 2015, *ApJL*, 811, L22. doi:10.1088/2041-8205/811/2/L22
- Just, O., Bauswein, A., Ardevol Pulpillo, R., et al. 2015, *MNRAS*, 448, 541. doi:10.1093/mnras/stv009
- Kasen, D., Badnell, N. R., & Barnes, J. 2013, *ApJ*, 774, 25. doi:10.1088/0004-637X/774/1/25
- Kasen, D., Metzger, B., Barnes, J., et al. 2017, *Nature*, 551, 80. doi:10.1038/nature24453
- Kawaguchi, K., Kyutoku, K., Shibata, M., et al. 2016, *ApJ*, 825, 52. doi:10.3847/0004-637X/825/1/52
- Kawaguchi, K., Shibata, M., & Tanaka, M. 2018, *ApJL*, 865, L21. doi:10.3847/2041-8213/aade02
- Kawanaka, N. & Mineshige, S. 2007, *ApJ*, 662, 1156. doi:10.1086/517985
- Kawanaka, N., Piran, T., & Krolik, J. H. 2013, *ApJ*, 766, 31. doi:10.1088/0004-637X/766/1/31
- Kiuchi, K., Sekiguchi, Y., Kyutoku, K., et al. 2015, *PhRvD*, 92, 064034. doi:10.1103/PhysRevD.92.064034
- Kohri, K. & Mineshige, S. 2002, *ApJ*, 577, 311. doi:10.1086/342166
- Kohri, K., Narayan, R., & Piran, T. 2005, *ApJ*, 629, 341. doi:10.1086/431354
- Korobkin, O., Rosswog, S., Arcones, A., et al. 2012, *MNRAS*, 426, 1940. doi:10.1111/j.1365-2966.2012.21859.x
- Kotake, K., Ohnishi, N., & Yamada, S. 2007, *ApJ*, 655, 406. doi:10.1086/509320
- Kotake, K., Sato, K., & Takahashi, K. 2006, *Reports on Progress in Physics*, 69, 971. doi:10.1088/0034-4885/69/4/R03
- Kotake, K., Takiwaki, T., & Harikae, S. 2012, *ApJ*, 755, 84. doi:10.1088/0004-637X/755/2/84
- Kyutoku, K., Ioka, K., Okawa, H., et al. 2015, *PhRvD*, 92, 044028. doi:10.1103/PhysRevD.92.044028
- Kyutoku, K., Ioka, K., & Shibata, M. 2013, *PhRvD*, 88, 041503. doi:10.1103/PhysRevD.88.041503
- Kyutoku, K. & Kashiyama, K. 2018, *PhRvD*, 97, 103001. doi:10.1103/PhysRevD.97.103001
- Lattimer, J. M. & Schramm, D. N. 1974, *ApJL*, 192, L145. doi:10.1086/181612
- Lee, W. H., Ramirez-Ruiz, E., & Page, D. 2005, *ApJ*, 632, 421. doi:10.1086/432373
- Lei, W. H., Wang, D. X., Zhang, L., et al. 2009, *ApJ*, 700, 1970. doi:10.1088/0004-637X/700/2/1970
- Lei, W.-H., Zhang, B., & Liang, E.-W. 2013, *ApJ*, 765, 125. doi:10.1088/0004-637X/765/2/125
- Li, A., Zhu, Z.-Y., Zhou, E.-P., et al. 2020, *Journal of High Energy Astrophysics*, 28, 19. doi:10.1016/j.jheap.2020.07.001
- Li, A., Zhu, Z.-Y., & Zhou, X. 2017, *ApJ*, 844, 41. doi:10.3847/1538-4357/aa7a00
- Li, L.-X. & Paczyński, B. 1998, *ApJL*, 507, L59. doi:10.1086/311680

- Li, L.-X., Zimmerman, E. R., Narayan, R., et al. 2005, *ApJS*, 157, 335. doi:10.1086/428089
- Lippuner, J., Fernández, R., Roberts, L. F., et al. 2017, *MNRAS*, 472, 904. doi:10.1093/mnras/stx1987
- Liu, T., Gu, W.-M., Xue, L., et al. 2007, *ApJ*, 661, 1025. doi:10.1086/513689
- Liu, T., Gu, W.-M., Xue, L., et al. 2012a, *Ap&SS*, 337, 711. doi:10.1007/s10509-011-0887-3
- Liu, T., Gu, W.-M., & Zhang, B. 2017a, *NewAR*, 79, 1. doi:10.1016/j.newar.2017.07.001
- Liu, T., Liang, E.-W., Gu, W.-M., et al. 2010, *A&A*, 516, A16. doi:10.1051/0004-6361/200913447
- Liu, T., Liang, E.-W., Gu, W.-M., et al. 2012b, *ApJ*, 760, 63. doi:10.1088/0004-637X/760/1/63
- Liu, T., Lin, C.-Y., Song, C.-Y., et al. 2017b, *ApJ*, 850, 30. doi:10.3847/1538-4357/aa92c4
- Liu, T., Lin, Y.-Q., Hou, S.-J., et al. 2015, *ApJ*, 806, 58. doi:10.1088/0004-637X/806/1/58
- Liu, T., Qi, Y.-Q., Cai, Z.-Y., et al. 2020, *ApJ*, in press, arXiv:2008.05087
- Liu, T., Song, C.-Y., Yi, T., et al. 2019, *Journal of High Energy Astrophysics*, 22, 5. doi:10.1016/j.jheap.2019.02.001
- Liu, T., Wei, Y.-F., Xue, L., et al. 2021, *ApJ*, 908, 106. doi:10.3847/1538-4357/abd24e
- Liu, T., Zhang, B., Li, Y., et al. 2016, *PhRvD*, 93, 123004. doi:10.1103/PhysRevD.93.123004
- Lyman, J. D., Lamb, G. P., Levan, A. J., et al. 2018, *Nature Astronomy*, 2, 751. doi:10.1038/s41550-018-0511-3
- Mandel, I., Müller, B., Riley, J., et al. 2021, *MNRAS*, 500, 1380. doi:10.1093/mnras/staa3390
- Margutti, R., Berger, E., Fong, W., et al. 2017, *ApJL*, 848, L20. doi:10.3847/2041-8213/aa9057
- Metzger, B. D. 2019, *Living Reviews in Relativity*, 23, 1. doi:10.1007/s41114-019-0024-0
- Metzger, B. D., Bauswein, A., Goriely, S., et al. 2015, *MNRAS*, 446, 1115. doi:10.1093/mnras/stu2225
- Metzger, B. D., Martínez-Pinedo, G., Darbha, S., et al. 2010, *MNRAS*, 406, 2650. doi:10.1111/j.1365-2966.2010.16864.x
- Metzger, B. D. & Piro, A. L. 2014, *MNRAS*, 439, 3916. doi:10.1093/mnras/stu247
- Müller, E. & Janka, H.-T. 1997, *A&A*, 317, 140
- Nakar, E. 2007, *PhR*, 442, 166. doi:10.1016/j.physrep.2007.02.005
- Nakar, E. 2020, *PhR*, 886, 1. doi:10.1016/j.physrep.2020.08.008
- Narayan, R., Paczyński, B., & Piran, T. 1992, *ApJL*, 395, L83. doi:10.1086/186493
- Narayan, R., Piran, T., & Kumar, P. 2001, *ApJ*, 557, 949. doi:10.1086/322267
- Oechslin, R. & Janka, H.-T. 2006, *MNRAS*, 368, 1489. doi:10.1111/j.1365-2966.2006.10238.x
- Paczynski, B. 1986, *ApJL*, 308, L43. doi:10.1086/184740
- Paczynski, B. 1991, *AcA*, 41, 257
- Perego, A., Radice, D., & Bernuzzi, S. 2017, *ApJL*, 850, L37. doi:10.3847/2041-8213/aa9ab9
- Piro, A. L. & Kollmeier, J. A. 2018, *ApJ*, 855, 103. doi:10.3847/1538-4357/aaaab3
- Popham, R., Woosley, S. E., & Fryer, C. 1999, *ApJ*, 518, 356. doi:10.1086/307259
- Rauch, K. P. & Blandford, R. D. 1994, *ApJ*, 421, 46. doi:10.1086/173625
- Rees, M. J. & Mészáros, P. 1992, *MNRAS*, 258, 41. doi:10.1093/mnras/258.1.41P
- Ren, J., Lin, D.-B., Zhang, L.-L., et al. 2019, *ApJ*, 885, 60. doi:10.3847/1538-4357/ab4188
- Romero, G. E., Reynoso, M. M., & Christiansen, H. R. 2010, *A&A*, 524, A4. doi:10.1051/0004-6361/201014882
- Safarzadeh, M. & Loeb, A. 2020, *ApJL*, 899, L15. doi:10.3847/2041-8213/aba9df
- Sathyaprakash, B. S. & Schutz, B. F. 2009, *Living Reviews in Relativity*, 12, 2. doi:10.12942/lrr-2009-2
- Savchenko, V., Ferrigno, C., Kuulkers, E., et al. 2017, *ApJL*, 848, L15. doi:10.3847/2041-8213/aa8f94
- Schutz, B. F. 1989, *Classical and Quantum Gravity*, 6, 1761. doi:10.1088/0264-9381/6/12/006
- Sekiguchi, Y., Kiuchi, K., Kyutoku, K., et al. 2011, *PhRvL*, 107, 051102. doi:10.1103/PhysRevLett.107.051102
- Siegel, D. M. & Metzger, B. D. 2017, *PhRvL*, 119, 231102. doi:10.1103/PhysRevLett.119.231102
- Song, C.-Y. & Liu, T. 2019, *ApJ*, 871, 117. doi:10.3847/1538-4357/aaf6ae
- Song, C.-Y., Liu, T., Gu, W.-M., et al. 2015, *ApJ*, 815, 54. doi:10.1088/0004-637X/815/1/54
- Song, C.-Y., Liu, T., & Li, A. 2018, *MNRAS*, 477, 2173. doi:10.1093/mnras/sty783
- Song, C.-Y., Liu, T., & Wei, Y.-F. 2020, *MNRAS*, 494, 3962. doi:10.1093/mnras/staa932
- Sun, M., Xue, Y., Trump, J. R., et al. 2019, *MNRAS*, 482, 2788. doi:10.1093/mnras/sty2885
- Sun, M.-Y., Liu, T., Gu, W.-M., et al. 2012, *ApJ*, 752, 31. doi:10.1088/0004-637X/752/1/31
- Surman, R., McLaughlin, G. C., Ruffert, M., et al. 2008, *ApJL*, 679, L117. doi:10.1086/589507
- Surman, R., McLaughlin, G. C., & Sabbatino, N. 2011, *ApJ*, 743, 155. doi:10.1088/0004-637X/743/2/155
- Suwa, Y. & Murase, K. 2009, *PhRvD*, 80, 123008. doi:10.1103/PhysRevD.80.123008

- Symbalisty, E. & Schramm, D. N. 1982, *Astrophys. Lett.*, 22, 143
- Tanaka, M. & Hotokezaka, K. 2013, *ApJ*, 775, 113. doi:10.1088/0004-637X/775/2/113
- Tanaka, M., Kato, D., Gaigalas, G., et al. 2018, *ApJ*, 852, 109. doi:10.3847/1538-4357/aaa0cb
- Tanaka, M., Kato, D., Gaigalas, G., et al. 2020, *MNRAS*, 496, 1369. doi:10.1093/mnras/staa1576
- Tanaka, M., Utsumi, Y., Mazzali, P. A., et al. 2017, *PASJ*, 69, 102. doi:10.1093/pasj/psx121
- Tanvir, N. R., Levan, A. J., Fruchter, A. S., et al. 2013, *Nature*, 500, 547. doi:10.1038/nature12505
- Troja, E., Piro, L., van Eerten, H., et al. 2017, *Nature*, 551, 71. doi:10.1038/nature24290
- Usov, V. V. 1992, *Nature*, 357, 472. doi:10.1038/357472a0
- Vieira, N., Ruan, J. J., Haggard, D., et al. 2020, *ApJ*, 895, 96. doi:10.3847/1538-4357/ab917d
- Villar, V. A., Guillochon, J., Berger, E., et al. 2017, *ApJL*, 851, L21. doi:10.3847/2041-8213/aa9c84
- Wanajo, S., Sekiguchi, Y., Nishimura, N., et al. 2014, *ApJL*, 789, L39. doi:10.1088/2041-8205/789/2/L39
- Warren, M. L., Couch, S. M., O'Connor, E. P., et al. 2020, *ApJ*, 898, 139. doi:10.3847/1538-4357/ab97b7
- Watson, A. M., Butler, N. R., Lee, W. H., et al. 2020, *MNRAS*, 492, 5916. doi:10.1093/mnras/staa161
- Wei, Y.-F. & Liu, T. 2020, *ApJ*, 889, 73. doi:10.3847/1538-4357/ab6325
- Wei, Y.-F., Liu, T., & Song, C.-Y. 2019, *ApJ*, 878, 142. doi:10.3847/1538-4357/ab2187
- Woosley, S. E. 1993, *ApJ*, 405, 273. doi:10.1086/172359
- Wu, M.-R., Barnes, J., Martínez-Pinedo, G., et al. 2019, *PhRvL*, 122, 062701. doi:10.1103/PhysRevLett.122.062701
- Wu, M.-R., Fernández, R., Martínez-Pinedo, G., et al. 2016, *MNRAS*, 463, 2323. doi:10.1093/mnras/stw2156
- Xue, L., Liu, T., Gu, W.-M., et al. 2013, *ApJS*, 207, 23. doi:10.1088/0067-0049/207/2/23
- Yang, B., Jin, Z.-P., Li, X., et al. 2015, *Nature Communications*, 6, 7323. doi:10.1038/ncomms8323
- Yu, Y.-W., Liu, L.-D., & Dai, Z.-G. 2018, *ApJ*, 861, 114. doi:10.3847/1538-4357/aac6e5
- Yu, Y.-W., Zhang, B., & Gao, H. 2013, *ApJL*, 776, L40. doi:10.1088/2041-8205/776/2/L40
- Yuan, F., Bu, D., & Wu, M. 2012b, *ApJ*, 761, 130. doi:10.1088/0004-637X/761/2/130
- Yuan, F., Gan, Z., Narayan, R., et al. 2015, *ApJ*, 804, 101. doi:10.1088/0004-637X/804/2/101
- Yuan, F. & Narayan, R. 2014, *ARA&A*, 52, 529. doi:10.1146/annurev-astro-082812-141003
- Yuan, F., Wu, M., & Bu, D. 2012a, *ApJ*, 761, 129. doi:10.1088/0004-637X/761/2/129
- Zevin, M., Spera, M., Berry, C. P. L., et al. 2020, *ApJL*, 899, L1. doi:10.3847/2041-8213/aba74e
- Zhang, B. 2018, *The Physics of Gamma-Ray Bursts* (Cambridge: Cambridge University Press). doi:10.1017/9781139226530
- Zhang, B. & Mészáros, P. 2001, *ApJL*, 552, L35. doi:10.1086/320255
- Zhu, J.-P., Wu, S., Yang, Y.-P., et al. 2021, arXiv:2106.15781
- Zhu, J.-P., Yang, Y.-P., Liu, L.-D., et al. 2020, *ApJ*, 897, 20. doi:10.3847/1538-4357/ab93bf